Available online at www.sciencedirect.com

SciVerse ScienceDirect

Procedia CIRP 5 (2013) 57 – 60

www.elsevier.com/locate/procedia

The First CIRP Conference on Biomanufacturing

Monitoring diameter and roundness errors in projection-microstereolithography of biomedical tooling and scaffolds

R. Bail*, J.I. Segal, S.M. Ratchev

Manufacturing Research Division, Faculty of Engineering, University of Nottingham, University Park, Nottingham NG7 2RD, U.K.

* Corresponding author. Tel.: +44-(0)115-956-6083 ; fax: +44-(0)115-951-3800 ; *E-mail address*: epxrb2@nottingham.ac.uk

Abstract

Projection-microstereolithography allows for great versatility in the design of biomedical components with round cross sections, such as fine strands, channels and microtubules. The working principle of this method, however, leads to a gradual accumulation of diameter and roundness errors following model approximation and part building. This study presents a method to monitor and quantify these inaccuracies, and the results demonstrate the challenges that emerge from building round microfeatures with this additive manufacturing technique and suggest the need for additional error compensation compared to non-round geometries.

Selection and/or peer-review under responsibility of Professor Mamoru Mitsuishi and Professor Paulo Bartolo

Keywords: Microstereolithography, photopolymerization, rapid tooling, scaffolds, micro-metrology.

1. Introduction

Projection-microstereolithography (PMSL) is a rapid-prototyping technique based on the spatially controlled solidification of a light-sensitive liquid polymer (photopolymerization) upon interaction with a light pattern generator, usually an LCD or a Digital Micromirror device (DMD), to digitally modulate a UV or visible light beam according to layer profiles determined from an STL file [1].

Novel applications for this technique arise in regenerative medicine with the need to mimic anatomical microenvironments for the regeneration of tissues. Microstereolithography is increasingly used to manufacture scaffolds in various designs and materials compatible with for example chondrocytes [2] or osteoblasts [3]. This technique also enables sophisticated biotooling design, such as bioreactors inspired by the microanatomy of vascular trees [4] or 3D cell culture environments for multiple cell types [5], as an alternative to conventional cell culturing methods.

These new applications benefit from design freedom provided by additive manufacturing techniques regarding the geometrical, hierarchical, functional and material complexity [6]. However, errors specific to the applied manufacturing software and equipment that affect part accuracy remain, and these can be classified into model approximation, part building and part finishing errors [7]. Originally suggested for scanning stereolithography, this classification can be adapted to other rapid-prototyping processes such as PMSL.

The accuracy of the model approximation is largely determined by the voxel size of the applied system in X/Y and Z direction. In PMSL, a layer profile is digitally represented by white ‘core pixels’ within the dimensions that match or are a multiple of the X/Y resolution, while areas that partly occupy a pixel may be represented by ‘fuzzy pixels’ in different gray scales depending on the pixel occupancy as shown in Fig. 1. Once an array of pixels is projected onto the resin surface, the accuracy of the part building process in each irradiated voxel is determined by material parameters and light-material interactions like the photosensitivity, penetration depth and shrinkage in the resin.

Selection and/or peer-review under responsibility of Professor Mamoru Mitsuishi and Professor Paulo Bartolo

doi:10.1016/j.procir.2013.01.011

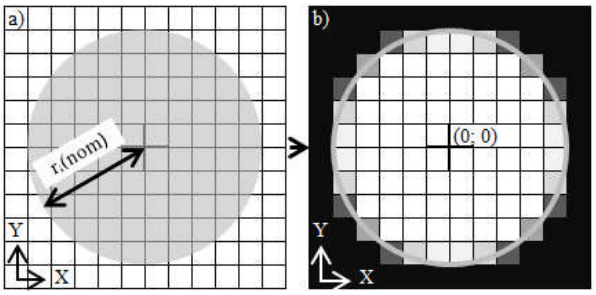

Fig. 1. (a) Sliced cylinder feature of nominal radius r_i(nom) against pixel grid applied by the machine software; (b) Approximation of a circular slice by white 'core pixels' and grayscale 'fuzzy pixels'.

Projection-microstereolithography is a powerful additive manufacturing technique to build biomedical microcomponents with complex geometries, but due to its functional principle it is challenging to accurately reproduce features with round cross sections, such as fine strands and microtubules, that can be highly relevant to these applications. This study presents a method to monitor and quantify the diameter and roundness errors for cylindrical features that occur after the different steps of a PMSL process. This will contribute to understanding the geometrical capability but also the additional challenges that emerge from building round features with this manufacturing technique compared to non-round geometries.

2. Materials and Methods

A test part containing arrays of cylindrical features with radii ranging from 10 to 250 micrometers (n=3) arranged on a 12 x 8 x 4 mm (L x W x H) base plate was designed in 'SolidWorks' CAD software. All dimensions in X/Y direction were a multiple of the X/Y-pixel size, while the feature height (Z) of 250 micrometers accounted for ten times the layer height applied in the stereolithography process. The CAD file was saved as a STL file and opened in the Envisiontec 'Perfactory RP' software suite to generate the sliced building data from these files that were used in the subsequent analysis and manufacturing process.

All test parts were built on a Envisiontec Perfactory® Mini-Multi Lens projection-microstereolithography machine in the Envisiontec 'RCP25' rapid-prototyping material. The projector brightness was calibrated to 600 mW/dm^2 and the exposure time for the standard range was set to 4 seconds per layer at a Z-resolution of 25 micrometers. The X/Y-resolution at 1050x1400 pixels (SXGA+) and deactivated enhanced resolution module was equivalent to a pixel size of 10x10 micrometers. The parts were cleaned post build in an ultrasonic isopropanol bath for 3 minutes and air-dried.

The sliced data information was recalled from the related JOB file and displayed in the Envisiontec 'Perfactory Job Modifier' software module. The mask image for the last layer showing the cross section of the cylinder arrays was then saved as a Portable Networks Graphics (PNG) file and displayed in 'ImageJ' image analysis software. The centre of each displayed circle was defined as the origin of each feature measurement (X=0; Y=0). The positions (X_i; Y_i) relative to the origin of the outermost pixel corner points were recorded for the 'core pixels' in white (n=3), and this was repeated for the 'fuzzy pixels' in the different gray shades.

The radius (r_i) at each measured point along the outer edge of the cylinder was calculated using the Pythagorean Theorem with the opposite (X_i) and the adjacent edge length (Y_i) as displayed in equation (1).

$$r_i = \sqrt{\Delta X_i^2 / \Delta Y_i^2} \tag{1}$$

The angles for each data point (X_i; Y_i) were calculated according to the inverse tangent (ATAN) as expressed in equation (2). The angle versus radius data sets were then plotted as roundness graphs for the different feature sizes after model approximation for both the radius following the outer line of the white pixels, r_i(w), and the radii along the edge of the gray pixels, r_i(g).

$$\alpha_i = ATAN \sqrt{\Delta X_i / \Delta Y_i} \times \frac{180}{\Pi} \tag{2}$$

The feature arrays were visually inspected on a Hitachi E-2600N scanning-electron microscope (SEM) in backscattered electron (BSE) mode, and a surface profile was generated via white-light interferometry on a Bruker NP Flex 3D Surface Metrology System. The metrological data for the produced test features was generated on a Zeiss F25 micro-Coordinate Measuring Machine (CMM) with a length measuring error of 250 nm (20°C), using a touch-trigger probe with a stylus of 120 µm diameter. Analogically to the model approximation error assessment, the centre point of each feature was defined as the datum, and data points (X_i; Y_i) were automatically taken along the circumferential lines at 150 micrometers height around each feature (n=3) at the according angles and in consistency with the resolution of the PNG file. Mean diameters and roundness after fabrication were calculated using the Gauss best-fit algorithm, based on the minimum sum of square distances (LSQ feature).

3. Results

3.1. Model approximation errors

With all feature radii, symmetry was observed in four directions with symmetry points at 0, 90, 180 and 270

degrees. An increase in the quality of the digital approximation was observed with increasing cylinder radii, whereas the quality of the reproduced circle images in particular with the smallest three radii remained poor. With all features except the smallest, a core zone of white pixels was surrounded by a narrow band of fuzzy pixels in different levels of gray determined by the pixel occupancy. Although the original CAD model contained cylinder features implying circular cross sections, the slices through the 50- and 40-micrometer cylinders were approximated in the used stereolithography software by octagon-like projections, the 30- and 20-micrometer radii resembled a cross pattern, and the smallest 10-micrometer cylinder was coarsely approximated by a square of 4 gray pixels as indicated in Fig. 2.

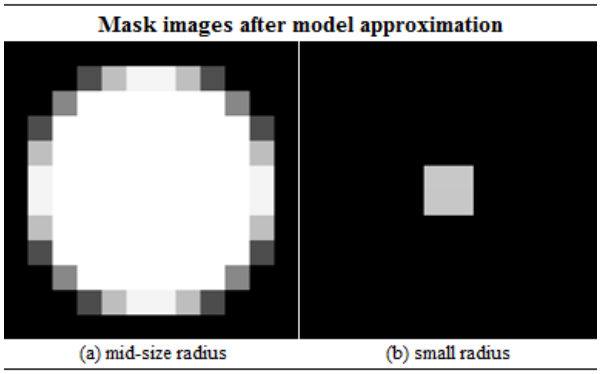

Fig. 2. Mask images after model approximation as displayed in the used image analysis software, (a) showing a cylinder of medium size (here the 50 µm radius) as octagon-like shape and (b) a small cylinder (here the 10 µm radius) represented by four gray pixels.

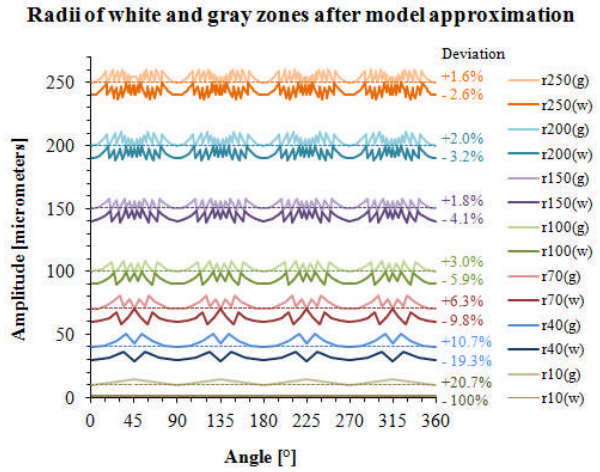

Fig. 3. Plots enclosing the core zones (white pixels, radii $r_i(w)$) and fuzzy zones (gray pixels, radii ($r_i(g)$) for different nominal cylinder radii after model approximation using Envisiontec 'Perfactory RP' software. Average deviations indicated in percent; 20, 30 and 50µm radii left out for clarity reasons.

As shown in Fig. 3, the radii $r_i(w)$ describing the outer edge of the white pixels did not exceed the according nominal radius $r_i(nom)$ but their average deviations generally increased with decreasing feature size from -2.6% for the 250-µm radius (r_{250}) over -9.8% for r_{70} down to -100% for the smallest feature r_{10}. For the radii $r_i(g)$ following the outer edge of the fuzzy pixels, the largest feature exhibited the smallest average radius deviation of +1.6% that gradually increased over +6.3% for $r_{70}(g)$ up to +20.7% for the smallest radius $r_{10}(g)$. Furthermore, the fuzzy radii $r_i(g)$ were equal to the nominal values at angles of 0, 90, 180 and 270 degrees.

The above plots illustrate that the radius deviations generally increased with smaller nominal values and that the white core pixel zones produced larger absolute deviations than the fuzzy zones of gray pixels, in particular for the cylinder features of 150µm and below 70µm. This suggests that the irradiation mask of the used stereolithography equipment slightly underdesigned round cylinder features. A limitation of the diagram in Fig. 3 is that it does not provide any information on the grayscale and resulting energy content of the fuzzy pixels. The measurements remain fuzzy so that conclusions regarding the diameter or roundness errors after model approximation are problematic at this stage.

3.2. Part building errors

The optical inspection of the test structure revealed that the geometrical capability of the applied stereolithography machine and resin to reproduce round features in X/Y direction was limited to diameters greater than a tenfold of the X/Y resolution of 10 micrometers of the used machine. It was merely possible to build cylinder features with the six largest radii from 50 to 250 micrometers, while the smaller features were not present in the fabricated part (Fig. 4).

While the informative value of the dimensional assessment after model approximation was compromised by the fuzzy outer pixels, the CMM measurements of the fabricated parts indicated a clearer result. Increasing deviations from the nominal radii were observed with decreasing cylinder size, ranging from -2.1% at the largest radius of 250 µm to -17.6% for the smallest measurable feature r_{70}, while an exceptionally high accuracy with almost no diameter error was observed for the cylinder feature with a radius of 200 µm. The smallest reproducible feature in the test setup of 50 µm radius could not be measured as it was too small and tapered to provide a surface required by the CMM. By contrast, overall good roundness was achieved will all features and a clear correlation between roundness errors and feature size was not recognizable as can be seen from the roundness errors displayed in Fig. 5.

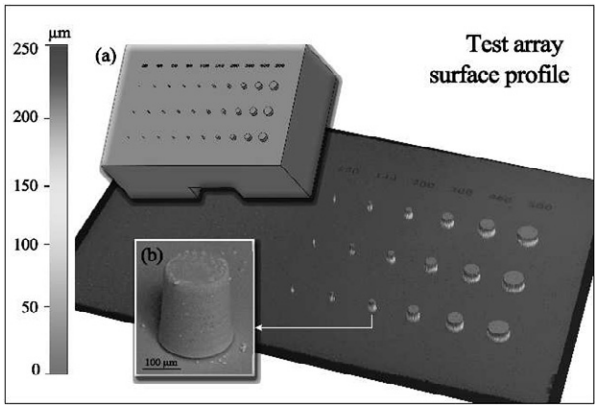

Fig. 4. Surface profile of the produced test array (interferometer) with feature height (Z) indicated by color shade on the scale bar, inset images showing (a) the CAD model and (b) a zoomed-in view (SEM) on the cylinder feature with a 200 µm diameter.

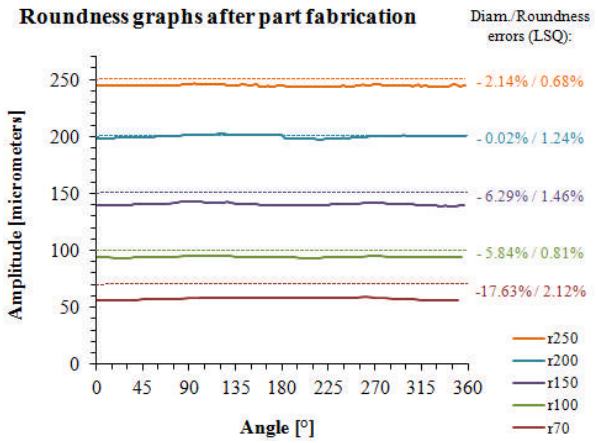

Fig. 5. Roundness graphs after part building for cylinders of large to intermediate size. Radii below 70 µm could not be measured, and small features with radii below 50 µm could not be reproduced with the applied stereolithography setup.

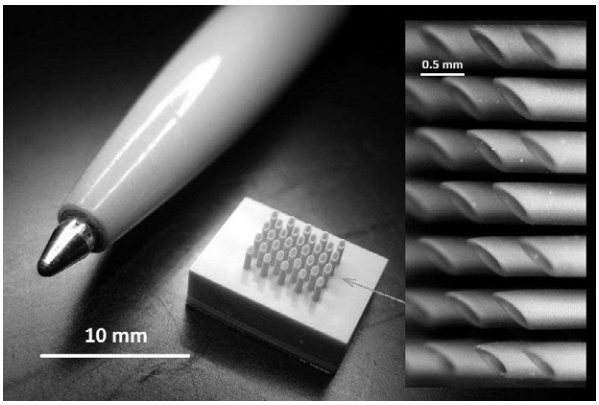

Fig. 6. Prototype of a 32-nozzle print head for cell deposition with a pitch of 1.2 mm and inner/outer nozzle diameters of 320/500 µm, inset image showing side view of the nozzle array with tapered tips.

The observed diameter errors may be the result of inaccuracies in the white and fuzzy zones of the light masks after model approximation and the material behavior, whereas the overall small roundness errors can be linked to the compensating effect of the gray pixels and a smoothening effect of the curing process on the feature surface. Minor oscillations in the roundness graphs might result from measuring errors and require further investigation. The gained data is useful to improve the diameter accuracy of round geometries by compensating for diameter errors in the design process. This understanding can be applied in the manufacture of biomedical micro components, with an example given in Fig. 6 showing a custom-designed, 32-nozzle print head with inner/outer nozzle diameters of 320/500 µm for the deposition of cell arrays.

4. Conclusions

The findings presented here suggest a method to quantify the diameter and roundness errors in a specific projection-microstereolithography process, which will contribute to increasing the accuracy and reproducibility in the manufacture of a wide range of biomedical micro-components using this additive technique.

Acknowledgements

The authors are grateful for the technical support provided by J. Straw and P. Wentworth from the *Precision Manufacturing Centre* at the University of Nottingham.

References

[1] Sun, C., Fang, N., Wu, D.M., Zhang, X., 2005. Projection micro-stereolithography using digital micro-mirror dynamic mask, Sensors and Actuators, A: Physical 121, p. 113.
[2] Lee, S.J., Kang, H.W., Park, J.K., Rhie, J.W., Hahn, S.K., Cho, D.W., 2008. Application of microstereolithography in the development of three-dimensional cartilage regeneration scaffolds, Biomedical Microdevices 10, p. 233.
[3] Melchels, F.P.W., Feijen, J., Grijpma, D.W., 2009. A poly(d,l-lactide) resin for the preparation of tissue engineering scaffolds by stereolithography, Biomaterials 30, p. 3801.
[4] Xia, C., Fang, N.X., 2009. 3D microfabricated bioreactor with capillaries, Biomedical Microdevices 11, p. 1309.
[5] Zorlutuna, P., Jeong, J.H., Kong, H., Bashir, R., 2011. Stereolithography-based hydrogel microenvironments to examine cellular interactions, Advanced Functional Materials 21, p. 3642.
[6] Gibson, I., Rosen, D.W., Stucker, B., 2010. Design for Additive Manufacturing, in: "*Additive Manufacturing Technologies*", I. Gibson, Editor. Springer Science+Business Media LLC, New York, p. 283.
[7] Pham, D.T., Ji, C., 2000. Design for stereolithography, Proceedings of the Institution of Mechanical Engineers, Part C: Journal of Mechanical Engineering 214, p. 635.